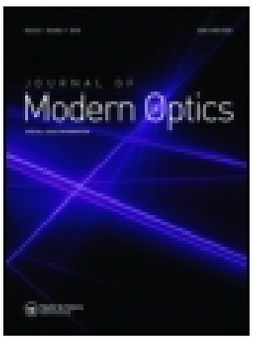

Journal of Modern Optics

ISSN: 0950-0340 (Print) 1362-3044 (Online) Journal homepage: http://www.tandfonline.com/loi/tmop20

Incoherent beam combining using fast steering mirrors

Guoqing Yang, Lisheng Liu, Zhenhua Jiang, Tingfeng Wang & Jin Guo

To cite this article: Guoqing Yang, Lisheng Liu, Zhenhua Jiang, Tingfeng Wang & Jin Guo (2016): Incoherent beam combining using fast steering mirrors, Journal of Modern Optics, DOI: 10.1080/09500340.2016.1229505

To link to this article: http://dx.doi.org/10.1080/09500340.2016.1229505

JOURNAL OF MODERN OPTICS, 2016
http://dx.doi.org/10.1080/09500340.2016.1229505

Taylor & Francis
Taylor & Francis Group

Incoherent beam combining using fast steering mirrors

Guoqing Yang[a,b], Lisheng Liu[a], Zhenhua Jiang[a], Tingfeng Wang[a] and Jin Guo[a]

[a]State Key Laboratory of Laser Interaction with Matter, Changchun Institute of Optics, Fine Mechanics and Physics, Chinese Academy of Science, Changchun, China; [b]University of Chinese Academy of Science, Beijing, China

ABSTRACT

Incoherent beam combining (ICBC) is a promising technique that can increase the total power of the lasers without decreasing the beam quality. Fast steering mirror (FSM) can be used in ICBC system to overlap the laser beams as well as suppress the jitter of the platform and the tip-tilt component of the turbulence. In this paper, a method using FSMs for incoherent beam combining is proposed and the relationship between the emergent light and the control voltages is derived, then the stochastic parallel gradient descent algorithm is adopted to calculate the optimal control voltages applied to the FSMs. A series of simulations combining two laser beams are carried on under static and dynamic turbulence. In order to verify the feasibility of this scheme, the dynamic turbulence is simulated under the hypothesis of Taylor's frozen turbulence. The results of simulations show that the turbulence would severely degrade the result of combining and the correction process would resist the influence and assure the evaluation function can reach the ideal situation at last. The model of the scheme used in this paper can be easily utilized for arbitrary amount of the lasers.

ARTICLE HISTORY
Received 18 April 2016
Accepted 19 August 2016

KEYWORDS
Laser beam combining; dynamic turbulence; SPGD algorithm; fast steering mirror

1. Introduction

Near-diffraction-limited beam quality is one of the most important characters of the laser in many fields such as national defence and industry. However, it has been proved that the output power and the beam quality are conflicted with each other, which means that it is impossible to increase the output power of a single fibre laser without decreasing the beam quality. Beam combining is one of the techniques proposed to mitigate such contradiction. Beam combining can be divided into coherent beam combing (CBC) and incoherent beam combining (ICBC); the primary difference between CBC and ICBC is whether there is an additional process for the precise phase locking of each laser. Owing to its advantages like compactness, robustness, high efficiency, lower maintenance and longer operating time compared to CBC, ICBC has received many attentions since it was proposed in the first place (*1*). A large number of methods for beam steering and combining have been proposed such as the adaptive fibre optics collimators (*2, 3*), active segmented mirror (*4*), diffraction gratings (*5*) and FSM (*1*). Among all of these methods, FSM is a promising instrument for beam overlapping and steering. The objective of ICBC technique is to achieve high output power, but almost all of the instruments mentioned above can't work regularly in the high power situation except FSM, besides, FSM also has advantages like rapid response speed and large operating frequency that are suited in the situation of real-time correction (*6*).

A position sensitive device (PSD) usually works with FSM to provide feedback signals through detecting position of light spot. However, a PSD is not available in the far-field applications, besides the light spots would be blurred and mixed due to atmospheric turbulence in which the tip-tilt component is more than 80% of the total aberrations according to the research of Noll (*7*). In this situation, the stochastic parallel gradient descent (SPGD) algorithm can be applied to calculate the proper control voltages of the FSMs for the correction process. SPGD algorithm, first used in beam correction by Vorontsov in 1997, has achieved great success because it can quickly find an extremum value for a system by adjusting control variables automatically (*8*). Compared to other algorithm that can be used for such situation like the genetic algorithm or the simulated annealing algorithm, the SPGD algorithm has proven to be much more efficient. In this paper, we propose a scheme in which feedback signals are acquired by detecting the distribution of the intensity in the target plane and then the SPGD algorithm is implemented to optimize the control voltages of the FSMs, thus generating ideal positions of the FSMs that can overlap the light spots appropriately and correct the majority tip-tilt aberrations of the atmospheric turbulence.

CONTACT Guoqing Yang yangguoqing13@mails.ucas.ac.cn

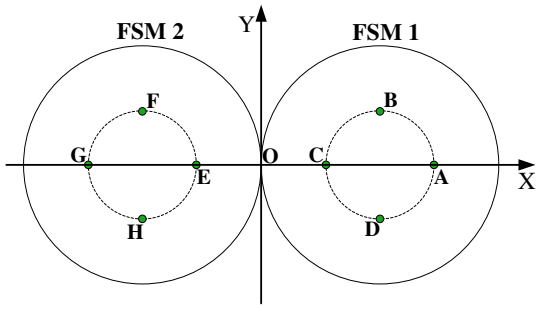

Figure 1. Geographical distribution of two FSMs (A, B, C, D, E, F, G, H are the locations of eight actuators).

To simplify the problem, we use two FSMs and two lasers for ICBC, but this model can be generalized for arbitrary lasers to be combined. The paper is organized as follows, Section 1 is the introduction to the background and the scheme used in our work; Section 2 is a brief review of the SPGD algorithm and the model we mentioned earlier; in Section 3, the simulation is carried on when there is no turbulence and static turbulence and the result is analysed; Section 4 brings out the simulation under dynamic turbulence and the result is compared with the one we got in Section 3; in Section 5, the conclusion is made.

2. Model using FSMs

2.1. Brief review of SPGD algorithm

The SPGD algorithm is derived by proposing a parallel method to estimate gradient of the function to calculate the extremum based on conventional gradient descent algorithm. Assume that the function can be written as: $F = F(x_1,x_2,\ldots,x_N)$, the maximum or the minimum can be reached when the variables change along the direction of the gradient. Unfortunately, not all functions have the analytical form, so the numerical method must be adopted to solve problems like that. The sequential perturbation technique and multidither technique are the common numerical methods, but the cost time of the traditional sequential perturbation technique and multidither technique would increase if the number of the control variables N increases (*9, 10*). Unlike the sequential perturbation and the multidither technique, SPGD algorithm generates a group of small perturbations $\left\{\delta x_j\right\}\ (j = 1, 2, \ldots N)$ firstly, making sure every item of $\left\{\delta x_j\right\}\ (j = 1, 2, \ldots N)$ has the same amplitude and random signs with equal probability. Adding the perturbations on the control variables and calculating the value of the function $F' = F\left(x_1 + \delta x_1, x_2 + \delta x_2, \ldots x_N + \delta x_N\right)$ in the next procedure. The variation between F' and $F(x_1,x_2,\ldots,x_N)$ can be expressed as $\delta F = F' - F = F\left(x_1 + \delta x_1, x_2 + \delta x_2, \ldots, x_N + \delta x_N\right) - F\left(x_1, x_2, \ldots, x_N\right)$ and then the gradient is written approximately

$$\frac{\partial F}{\partial x_i} = \frac{\delta F}{\delta x_i} \tag{1}$$

Let γ be the gain coefficient, when the value of γ is well set, the amplitude of the gradient can be expressed as $\delta F \delta x_i$. Then the control variables can be updated along the direction of the gradient

$$x_i^{(n+1)} = x_i^{(n)} + \gamma \left|\delta x_i\right| \delta F \tag{2}$$

where $\gamma > 0$ for the maximum of the function and $\gamma < 0$ for the minimum of the function, n is the iterative number. As the iterative number n increases, the maximum (or the minimum) of the function can be found at certain point $(x_1{}^n, x_2{}^n, \ldots, x_N{}^n)$.

2.2. Model for ICBC using FSMs

The geographical distribution of two FSMs is showed in Figure 1. The radius of the FSM is assumed to be r and *A, B, C, D* represent the positions of four actuators of FSM1 (*E, F, G, H* are positions of actuators of FSM2). The coordinates of the eight actuators in the coordinate system showed in Figure 1**.** can be written as:

A (1.464r, 0); B (r, 0.464r); C (0.536r, 0); D (r, –0.464r)
E (–0.536r, 0); F (–r, 0.464r); G (–1.464r, 0); H (–r, –0.464r)

The mirror is assumed to be rigid, each FSM can be driven using only two voltages V_x and V_y. Let s_0 represents the length change of the actuator change when 1 unit voltage is applied. The change of the mirror in the x and y direction can be expressed as:

$$\begin{aligned} z_x &= \frac{V_x s_0}{0.464r} x \\ z_y &= \frac{V_y s_0}{0.464r} y \end{aligned} \tag{3}$$

The total change in the mirror can be then expressed as the sum of z_x and z_y,

$$z = z_x + z_y = \frac{s_0}{0.464r}\left(V_x x + V_y y\right) \tag{4}$$

Considering one FSM, we set the coordinate system in the centre of the FSM, all of the control voltages are zero, the incident wavefront takes the form of Gauss beam, which is

$$A_0 = a_0 e^{\left[\frac{-\left(x^2+y^2\right)}{2w_0^2}\right]} e^{\left[ik\left(y\cos\left(\frac{3\pi}{4}\right)+z\cos\left(\frac{\pi}{4}\right)\right)\right]} \tag{5}$$

The reflected wavefront can be written as

$$A_r = a_0 e^{\left[\frac{-\left(x^2+y^2\right)}{2w_0^2}\right]} e^{\left[ik\left(y\cos\left(\frac{\pi}{4}\right)+z\cos\left(\frac{\pi}{4}\right)\right)\right]} \tag{6}$$

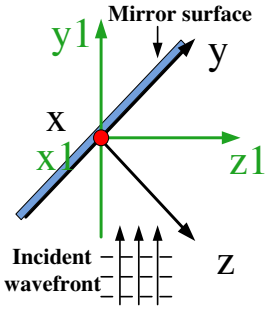

Figure 2. The coordinate system set on the FSM (*x*, *y*, *z*) and the coordinate system of the propagation (*x*1, *y*1, *z*1).

Table 1. Parameters used in the simulations.

Parameter	Value
Propagation distance: L	500 m
Wavelength: λ	532 nm
Beam waist: ω_0	5 mm
Radius of the FSM: r	12.5 mm
Sampling number: N	512
Coherent length of atmosphere: r_0	10 cm, 8 cm, 5 cm

The relationship between the control voltages and the tilt angles of the mirror θ_x and θ_y can be deduced from the geometry

$$\begin{aligned}\cos\left(\theta_x\right) &= \frac{s_0}{0.464r\sqrt{1+\left(\frac{s_0}{0.464r}\right)^2\left(V_x^2+V_y^2\right)}}\left|V_x\right| \\ &= \frac{s_0}{\sqrt{(0.464r)^2+s_0^2\left(V_x^2+V_y^2\right)}}\left|V_x\right|\end{aligned} \tag{7}$$

$$\begin{aligned}\cos\left(\theta_y\right) &= \frac{s_0}{0.464r\sqrt{1+\left(\frac{s_0}{0.464r}\right)^2\left(V_x^2+V_y^2\right)}}\left|V_y\right| \\ &= \frac{s_0}{\sqrt{(0.464r)^2+s_0^2\left(V_x^2+V_y^2\right)}}\left|V_y\right|\end{aligned} \tag{8}$$

In the coordinate system shown in Figure 2, when the mirror rotated at angle α around the x-axis, the reflected wavefront rotated 2α. When the mirror rotated at angle θ around the y-axis, the reflected wavefront rotated $\sqrt{2}\theta$ (*11*).

The equation of the reflect wavefront under the circumstance when the mirror is deflected at angles θ_x and θ_y in the direction of x-axis and y-axis separately can be derived from former analysis

$$A_r = a_0 e^{\left[\frac{-\left(x^2+y^2\right)}{2w_0^2}\right]} e^{\left[ik\left(x\cos\left(\frac{\pi}{2}+2\theta_x\right)+y\cos\left(\frac{\pi}{4}+\sqrt{2}\theta_y\right)+z\cos\left(\frac{\pi}{4}\right)\right)\right]} \tag{9}$$

Conversion of the coordinates must be taken into consideration when the coordinate system moves from (*x*, *y*, *z*) to (x_1, y_1, z_1) as shown in Figure 2. The spin matrix is

$$R = \begin{pmatrix} 1 & 0 & 0 \\ 0 & \cos\varphi & -\sin\varphi \\ 0 & \sin\varphi & \cos\varphi \end{pmatrix} \tag{10}$$

where $\varphi = \pi/4$ is the angle between z-axis and z_1-axis. Then the reflected wavefront changes its form

$$A_r = U_0 e^{\left[ik\left(x\cos\left(\frac{\pi}{2}+2\theta_x\right)+\frac{y+z}{\sqrt{2}}\cos\left(\frac{\pi}{4}+\sqrt{2}\theta_y\right)+\frac{z-y}{\sqrt{2}}\cos\left(\frac{\pi}{4}\right)\right)\right]} \tag{11}$$

$$U_0 = a_0 e^{\left[\frac{-\left[2x^2+(y+z)^2\right]}{4w_0^2}\right]} \tag{12}$$

We extend the model to situation where two FSMs are used, the reflected wavefront can be written separately as:

$$A_{r1} = U_1 e^{\left[ik\left((x-x1)\cos\left(\frac{\pi}{2}+2\theta_x\right)+\frac{y+z}{\sqrt{2}}\cos\left(\frac{\pi}{4}+\sqrt{2}\theta_y\right)+\frac{z-y}{2}\right)\right]} \tag{13}$$

$$U_1 = a_0 e^{\left[\frac{-\left[2(x-x1)^2+(y+z)^2\right]}{4w_0^2}\right]} \tag{14}$$

$$A_{r2} = U_2 e^{\left[ik\left((x-x2)\cos\left(\frac{\pi}{2}+2\theta_x\right)+\frac{y+z}{\sqrt{2}}\cos\left(\frac{\pi}{4}+\sqrt{2}\theta_y\right)+\frac{z-y}{2}\right)\right]} \tag{15}$$

$$U_2 = a_0 e^{\left[\frac{-\left[2(x-x2)^2+(y+z)^2\right]}{4w_0^2}\right]} \tag{16}$$

3. Simulations without turbulence and under static turbulence

3.1. Simulation without turbulence

The parameters used in simulation are listed in Table 1.

The feedback device used in this paper is assumed to be a conventional CCD. The CCD which located in the transmitter plane would acquire the image of the intensity distribution in the target plane. Then the merit function is analysed based on the image.

The intensity distribution in the target plane when the lasers propagate in the free space without turbulence is shown in Figure 3(a).

The distribution of light spots after correction is shown in Figure 3(b). It can be inferred from the two pictures easily that the power after correction is twice as stronger than the one before correction, besides, the light spot after correction can still maintain the near-diffraction limit beam quality. We adopt the image sharpness function as the evaluation function to appraise the correction process. The sharpness function is defined below

$$J = \iint I^2(x,y)\,\mathrm{d}x\mathrm{d}y \tag{17}$$

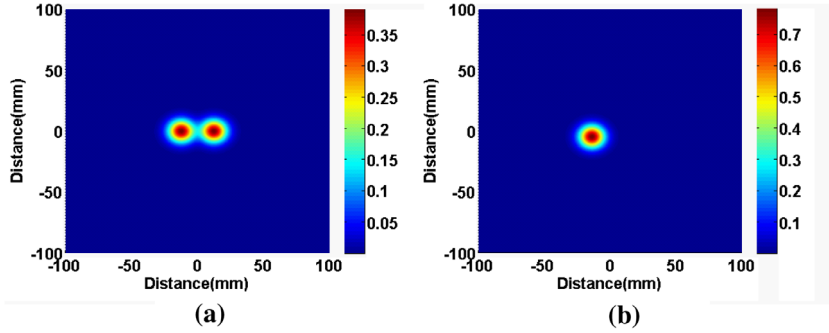

Figure 3. (a): The light spots distribution in the target plane without correction process; (b): The light spots distribution in the target plane after correction process.

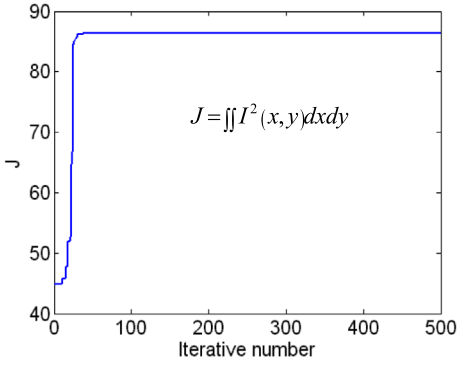

Figure 4. Evaluation function J against iterative number during the correction process.

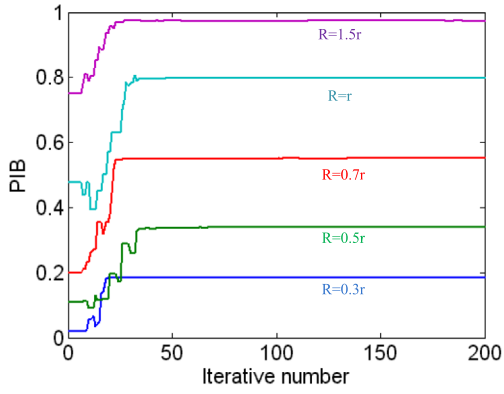

Figure 5. PIB value against iterative number with different R.

$I(x, y)$ is the intensity distribution in the target plane. The relationship between the evaluation function J and the iterative number is shown in Figure 4. When the iterative number is under 100, the evaluation function increases rapidly as the iterative number increases and becomes stable subsequently. The power in the bucket (PIB) index, one of the most important parameters in high energy laser applications, is the total power inside a circle with radius of R. PIB indicates the concentration degree of the energy. The definition of PIB is shown in Equation (18).

$$PIB = \frac{\int_0^{2\pi}\int_0^{R} I(r,\theta) r \mathrm{d}r\mathrm{d}\theta}{\int_0^{2\pi}\int_0^{\infty} I(r,\theta) r \mathrm{d}r\mathrm{d}\theta} \tag{18}$$

where $I(r, \theta)$ is the intensity distribution written in polar coordinates, R is the radius of the PIB.

The curve of PIB value against iterative number during the correction process is illustrated in Figure 5, r is the radius of the mirror. The radius of the light spot in the target plane is about $1.4r$ in the ideal situation according to the physical optics theory; the curves in Figure 5 have the same trend for different R. When $R = 1.5r$, PIB value is about 0.98 when stabilized. The SPGD algorithm achieves an excellent result for ICBC under the circumstance without turbulence.

3.2. Simulation with static turbulence

In a system that used in far-field situation, the atmospheric turbulence is the most severe problem. The simulation under static turbulence is performed using split-step beam propagation method in which the phase screens are generated through power spectrum method based on fast Fourier transform. The intensity distribution shown in Figure 6(a)–(c) is the consequence of initial Gauss beams that propagate through static atmospheric turbulence without correction. The coherent lengths of atmosphere in Figure 6(a)–(c) are 10, 8 and 5 cm separately. Smaller coherent length indicates stronger turbulence, the light spots in the target plane becomes more and more irregular as the coherent length decreases.

Figure 6(d)–(f) are the corresponding results of Figure 6(a)–(c) with correction. It can be inferred that

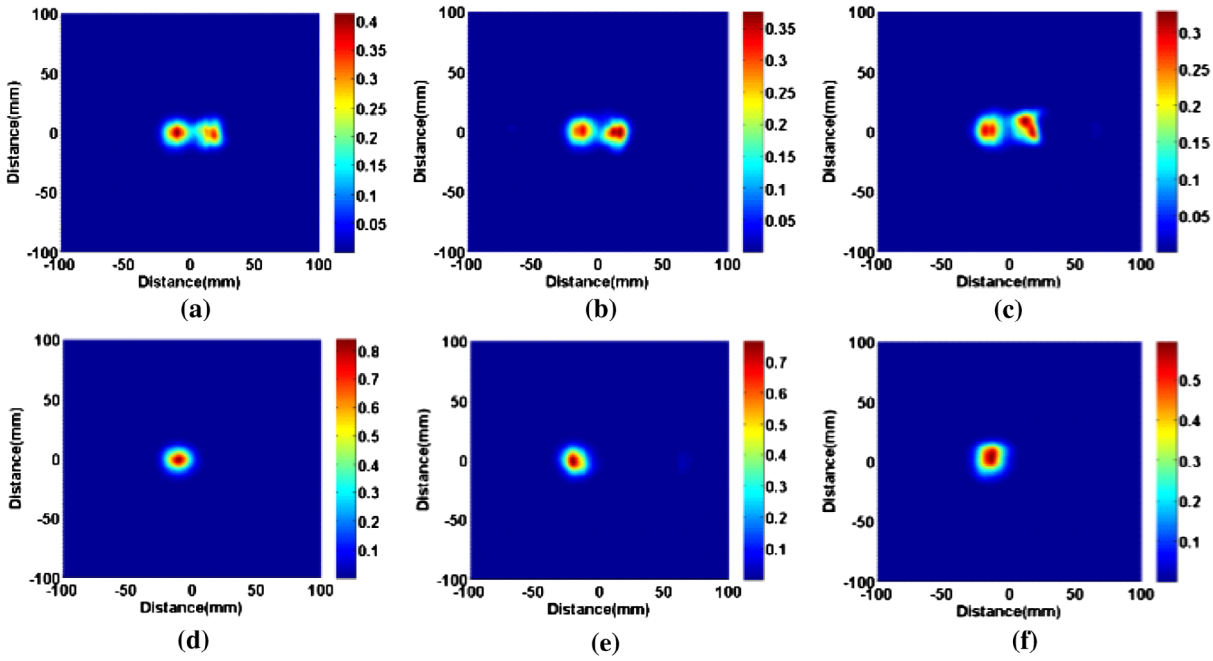

Figure 6. (a), (b), (c): The light spot distribution in target plane under different coherent lengths before correction. (a): 10 cm; (b): 8 cm; (c): 5 cm. (d), (e), (f): The corresponding results after correction of (a), (b), (c).

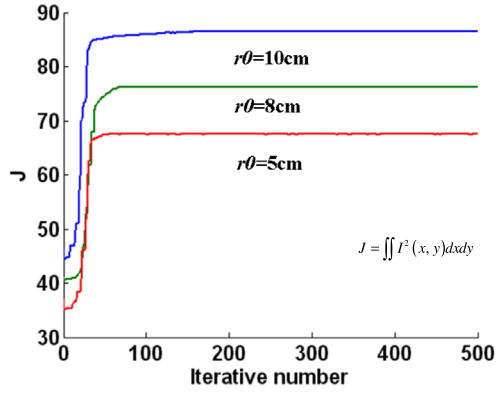

Figure 7. Evaluation function J against iterative number under different strengths of turbulence.

this method is still able to achieve a good result even there exists static turbulence.

Figure 7 shows the evaluation function against iterative number under different coherent lengths of atmosphere r_0. Compared with Figure 4, the curves have a little vibration due to the atmosphere after the iterative number reaches 100, besides, the correction result under big coherent length (weak turbulence) is much better than the result under small coherent length (strong turbulence). The PIB value in Figure 8 indicates that the proposed method is feasible even the turbulence is strong. On comparing different curves in Figure 8, it can be seen that although the coherent lengths r_0 are different, the combining efficiencies are close to each other when the radiuses are the same. The reason for that is the turbulence doesn't expand the beam too much except for a little flare surrounding the spot that has limited influence on the PIB value.

4. Simulations under dynamic turbulence

The most important assumption used in the former section is that the turbulence is stillness. However, as we all know, the turbulence is dynamic in real-time. It is important to find a method to simulate the dynamic turbulence and validate the effectiveness of the proposed method under dynamic turbulence.

Taylor's hypothesis of frozen turbulence is used here to simulate the dynamic turbulence (*12*). The hypothesis states that temporal variations in meteorological quantities at a point are produced by the mean wind speed flow and not by changes in the quantities themselves. Under the hypotheses, the wind speed is expressed as V and the phase that caused by turbulence at certain point r when the time is $t + \tau$ can be expressed by the phase at point $r - V\tau$ at time t, the relationship can be written as

$$p(r, t + \tau) = p(r - V\tau, t) \tag{19}$$

where p denotes the phase caused by turbulence. For the simulation of dynamic turbulence, the phase screens whose sizes are $4N \times 4N$ are generated firstly, where N is the number of pixel at the incident plane. The wind speed

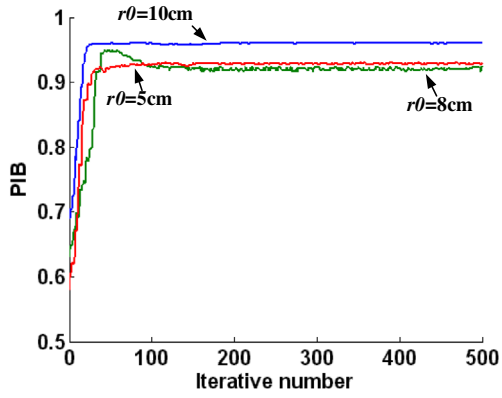

Figure 8. PIB value against iterative number with the same radius $R = 1.5r$ for different atmosphere turbulences.

is assumed to be V, the aperture in the incident plane is D and the bandwidth of the system is f_0. The shift of pixels in phase screens for each iteration can be calculated from the parameters given above

$$V_s = \frac{N}{D}\frac{V}{f_0} \tag{20}$$

All the phase screens move at the same speed and direction. The simulation under dynamic turbulence is carried out using the method mentioned above. The intensity distribution is illustrated in Figure 9. Figures 9(a)–(c) are the intensity distributions without correction. The pattern of the distribution is dynamic and the light spots of two beams can hardly be extracted from each other. Even though the distribution in Figure 9(c) shows the light spots are merged already, the pattern cannot hold steady. Figure 10 shows the evaluation function and the PIB curve during the dynamic turbulence without correction. The evaluation function and PIB fluctuate as the phase screens move. We can infer from Figure 10 the process without correction is extremely unstable and it will become more difficult for system to correct. Figure 9(d)–(f) show the change in distribution of intensity, from which we can see this method still works well for dynamic turbulence.

The evaluation function J and the PIB value against iterative number under correction process are shown in Figure 11. As the figure shows, the evaluation function and PIB value can achieve a good result after correction, although the entire process is vibrating due to the influence of dynamic turbulence and the mean values are acceptable.

The numerical results of the above simulations are shown in Tables 2 and 3. All the values are normalized, the coherent length of static and dynamic turbulence is 10 cm. The evaluation function can reach the value of ideal situation when there is no turbulence or under static turbulence, but the dynamic turbulence which has the same strength with static turbulence would degrade the result

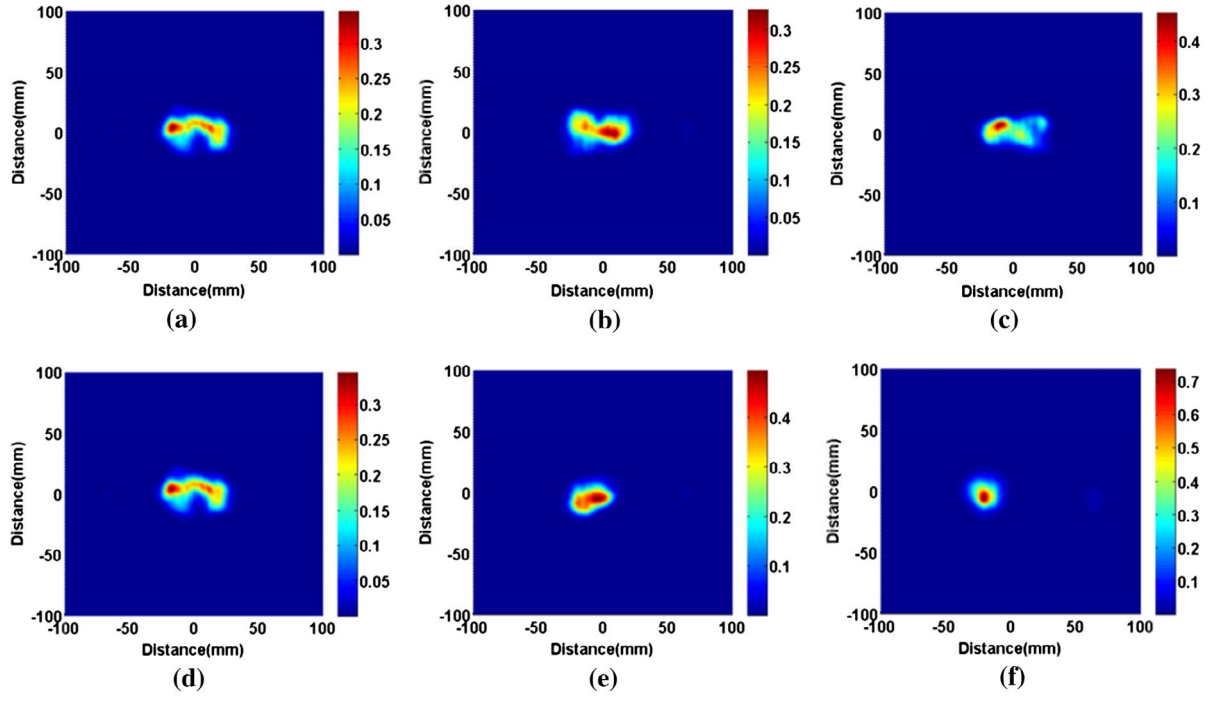

Figure 9. (a), (b), (c): Light spots distribution in the target plane under dynamic turbulence at different time without correction; (d), (e), (f): Light spots distribution in the target plane under dynamic turbulence at different time with correction.

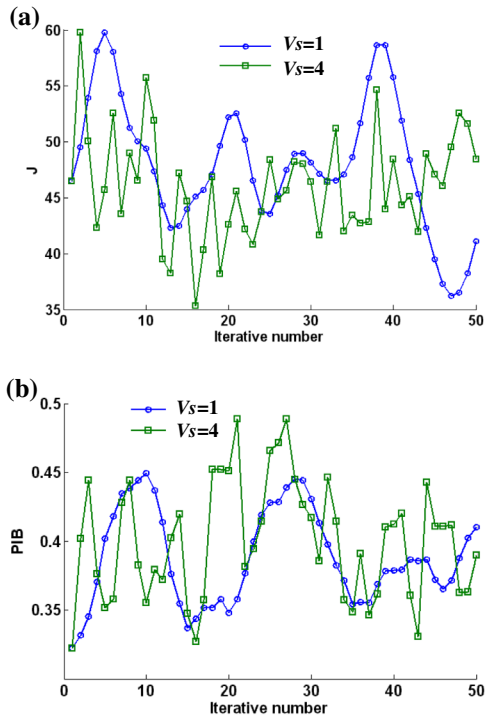

Figure 10. (a): Evaluation function against iterative number without correction; (b): PIB value against iterative number without correction.

Table 2. The stabilized value of evaluation function and its standard deviation for different simulations.

	Stabilized value of evaluation function	Standard deviation
Without turbulence	0.99	0.0054
Static turbulence	0.99	0.1134
Dynamic turbulence	0.93	5.7445

Table 3. The stabilized value of PIB and its standard deviation for different simulations.

	Stabilized value of PIB	Standard deviation
Without turbulence	0.9988	4.7731e-06
Static turbulence	0.9598	2.7546e-04
Dynamic turbulence	0.8052	0.0218

remains stable as long as the fluctuations are inside the circle. So it is proper to choose the PIB value as the index to assess the system exposed in the atmosphere.

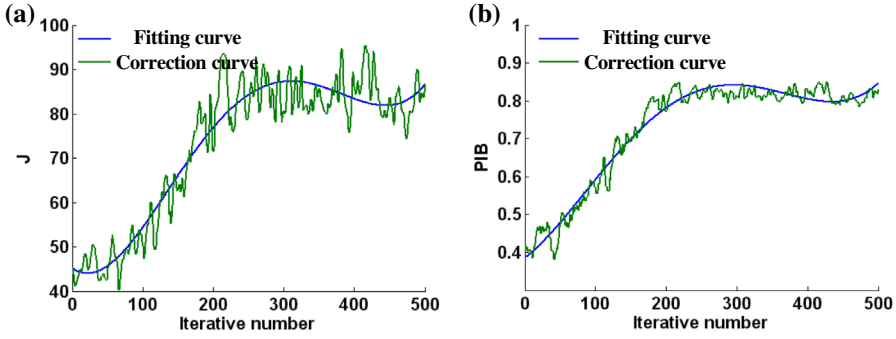

Figure 11. (a): Evaluation function against iterative number with correction; (b): PIB value against iterative number with correction.

of correction. Same conclusion is obtained from Table 3. The wind has a severe impact on ICBC, because the gradient of the former situation calculated by the algorithm has already been changed by wind, the wind has already changed the gradient. According to the standard deviations in Tables 2 and 3, PIB value has a smaller standard deviation than the sharpness function, which means that PIB value is more stable than the sharpness function that can be less influenced by the turbulence. This is because the second power of the intensity distribution presents the sharpness function, which would sharply fluctuate as the intensity distribution vibrates due to turbulence. However, the PIB which represents the total power inside a circle

5. Conclusion

In this paper, a method for beam steering and correction of tip-tilt component using SPGD algorithm and FSMs for ICBC is proposed. This method is verified though simulation in free-space and with static turbulence. After correction, the maximum power in the target plane doubles. The combining efficiency under different strengths of turbulence is also analysed. Also, the dynamic turbulence is simulated using Taylor's hypothesis of frozen turbulence, the results of evaluation function and PIB value are analysed which indicate that the scheme can achieve a promising result for incoherent beam combing under the

dynamic turbulence. Finally, the reason why the dynamic turbulence would influence the correction process is discussed and the data obtained under different simulations are analysed and discussed.

Disclosure statement

No potential conflict of interest was reported by the authors.

References

(1) Sprangle, P.; Ting, A.; Penano, J.; Fischer, R.; Hafizi, B. Incoherent Combining and Atmospheric Propagation of High-power Fiber Lasers for Directed-energy Applications. *IEEE J. Quantum Electron.* **2009**, *45*, 138–148.

(2) Beresnev, L.A.; Vorontsov, M.A. Design of Adaptive Fiber Optics Collimator for Free-space Communication Laser Transceiver. *Opt. Photonics*, **2005**, 5895, 58950R–58950R-7.

(3) Zhi, D.; Ma, P.; Ma, Y.; Wang, X.; Zhou, P.; Si, L. Novel Adaptive Fiber-optics Collimator for Coherent Beam Combination. *Opt. Express* **2014**, *22*, 31520–31528.

(4) Y. Tan, X.Li, W.Luo, C.Geng, Numerical analysis of the convergence speed of the SPGD algorithm with two different perturbation methods in coherent beam combination using active segmented mirror, in XX International Symposium on High Power Laser Systems and Applications, Chengdu China, **2015**.

(5) Wirth, C.; Schmidt, O.; Tsybin, I.; Schreiber, T.; Peschel, T.; Brückner, F.; Clausnitzer, T.; Limpert, J.; Eberhardt, R.; Tünnermann, A.; Gowin, M.; Have, E. ten.; Ludewigt, K.; Jung, M. 2 kW Incoherent Beam Combining of Four Narrow-linewidth Photonic Crystal Fiber Amplifiers. *Opt. Express* **2009**, *17*, 1178–1183.

(6) Kudryashov, A.; Alexandrov, A.; Rukosuev, A.; Samarkin, V.; Galarneau, P.; Turbide, S.; Châteauneuf, F. Extremely High-power CO_2 Laser Beam Correction. *Appl. Opt.* **2015**, *54*, 4352–4358.

(7) Noll, R.J. Zernike Polynomials and Atmospheric Turbulence. *J. Opt. Soc. Am.* **1976**, *66*, 207–211.

(8) Vorontsov, M.A.; Carhart, G.W.; Ricklin, J.C. Adaptive Phase-distortion Correction Based on Parallel Gradient-descent Optimization. *Opt. Lett.* **1997**, *22*, 907–909.

(9) Muller, R.A.; Buffington, A. Real-time Correction of Atmospherically Degraded Telescope Images Through Image Sharpening. *J. Opt. Soc. Am.* **1974**, *64*, 1200–1210.

(10) O'Meara, T.R. The Multidither Principle in Adaptive Optics. *J. Opt. Soc. Am.* **1977**, *67*, 306–315.

(11) Born, M.; Wolf, E. *Principles of Optics* **1999**, *1*, 38–58.

(12) Andrews, L.C.; Phillips, R.L. *Laser Beam Propagation through Random Media*; SPIE press, Bellingham, WA, **2005**; Vol. 1.